Supplementary Information

Flexible pH sensors based on OECTs with BTB dye embedded ion-gel gate dielectric

Xin Chen,[a] Jianlong Ji,*[,b,c] Yubo Peng,[d] Zhipeng Gao,[d] Min Zhao,[e] Bin Tang,*[,a] and Ying Liu *[,a]

[a] College of Materials Science and Engineering, Taiyuan University of Technology, Taiyuan 030024, China;

[b] College of Information and Computer, Taiyuan University of Technology, Taiyuan 030024, China;

[c] School of Integrated Circuits, Tsinghua University, Beijing 100084, China;

[d] College of Biomedical Engineering, Taiyuan University of Technology, Taiyuan 030024, China;

[e] Key Laboratory of Interface Science and Engineering in Advanced Materials Ministry of Education, Taiyuan University of Technology, Taiyuan 030024, China.

* Corresponding authors.

E-mail: liuying01@tyut.edu.cn (Y. Liu); tangbin@tyut.edu.cn (B. Tang);
jijianlong@tyut.edu.cn (J. Ji).

1. Schematic diagram of two chip device structures

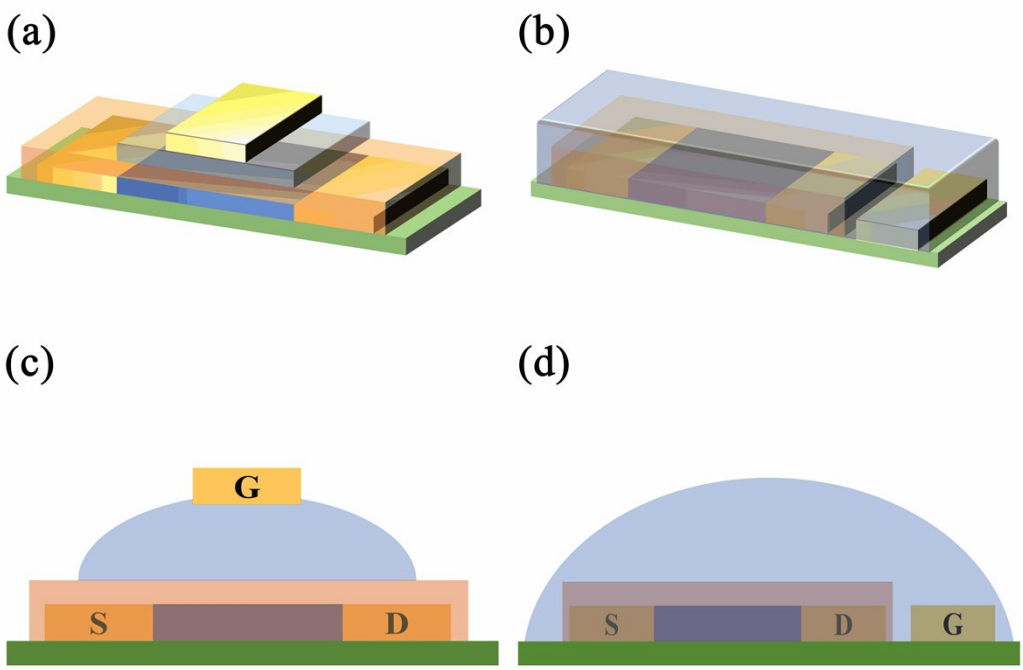

Figure S1 Schematic diagram of two chip device structures. (a) (c) Rigid organic electrochemical transistor (OECT), (b) (d) Flexible OECT.

2. I-V curves of the OECT

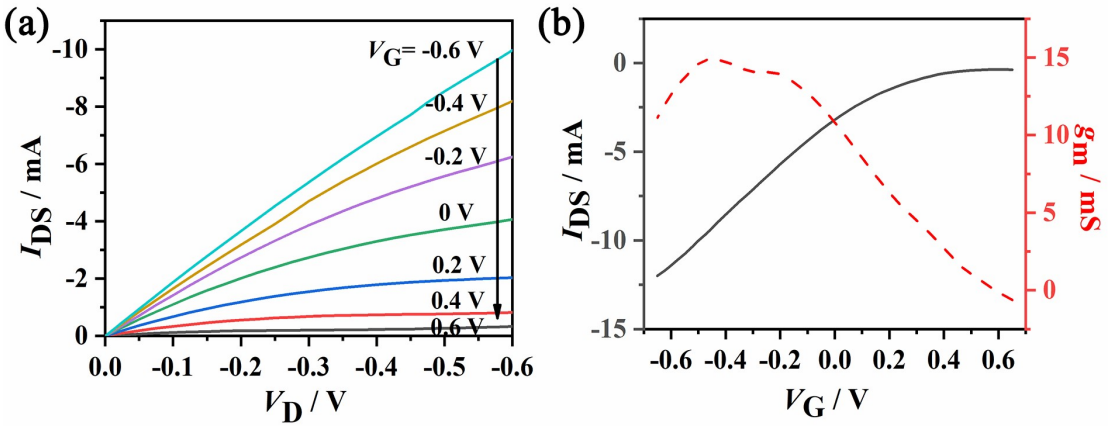

Figure S2 (a) Output curves of OECT, (b) Transfer and trans-conductance curves.

Figure S2 shows the results of transfer and output performance tests of rigid devices with 15 wt.% BTB ion-gel as a dielectric layer. In order to demonstrate the performance of the device itself, 0.1 M NaCl solution was used here as the liquid electrolyte for testing.

3. Sensitivity of pH sensors

Table S1 The sensitivity of pH sensors to the changes in Bromothymol blue (BTB) content and gate voltages (μA·dec^{-1})

BTB content	V_G / V				
	+0.4	+0.2	-0.2	-0.4	-0.6
0 wt.%	5.2 ± 1.2	11.2 ± 3.5	28.9 ± 2.5	43.1 ± 5.9	33.0 ± 3.2
5 wt.%	8.4 ± 0.9	18.9 ± 2.1	31.4 ± 3.2	51.2 ± 4.0	25.2 ± 4.6
10 wt.%	28.3 ± 4.3	70.0 ± 4.7	409.5 ± 51.3	446.0 ± 58.4	295.1 ± 33.2
15 wt.%	96.0 ± 20.5	111.7 ± 12.7	462.3 ± 72.9	622.1 ± 66.6	308.7 ± 61.7
20 wt.%	10.2 ± 1.9	34.4 ± 5.6	119.1 ± 11.3	202.2 ± 37.7	181.5 ± 54.2

4. The transfer curves of the OECT at different pH solutions

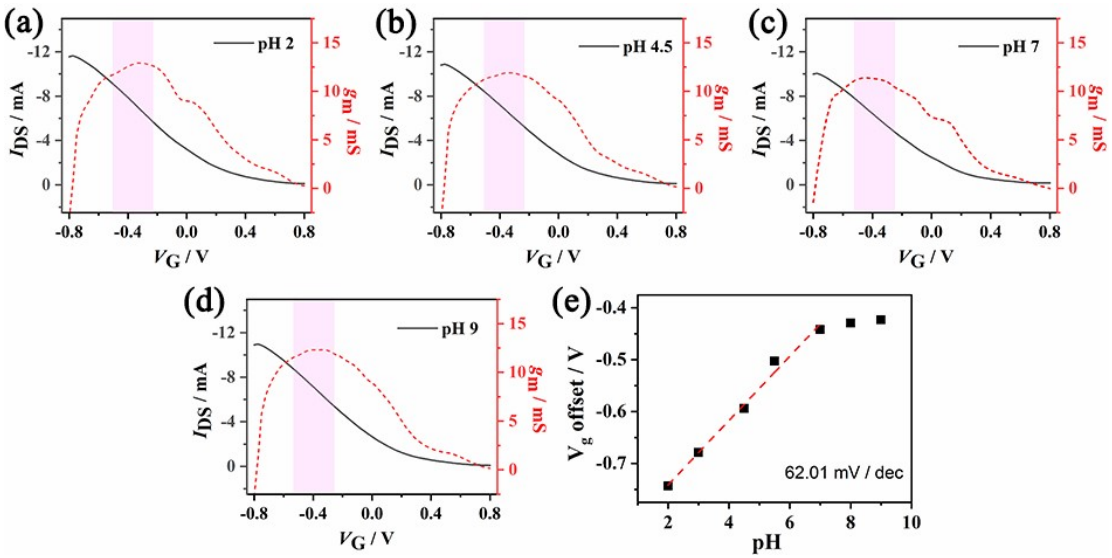

Figure S3 The transfer curves of the 15 wt.% ion-gel modified OECT at different pH solutions. (a) pH 2, (b) pH 4.5, (c) pH 7, (d) pH 9, and (e) Super-Nernstian sensitivity

Fig. S3(e) shows the voltage sensitivity of 15 wt.% BTB of ion-gel OECT at V_G= -0.4 V. We use the pH 7 transfer curve as a benchmark for the calculation. Finally, the minimum voltage sensitivity is obtained as 62 mV·dec^{-1} (> 55.9 mV·pH^{-1}).

5. The diagram of the relationship between transduction and BTB contents at V_G= -0.4 V

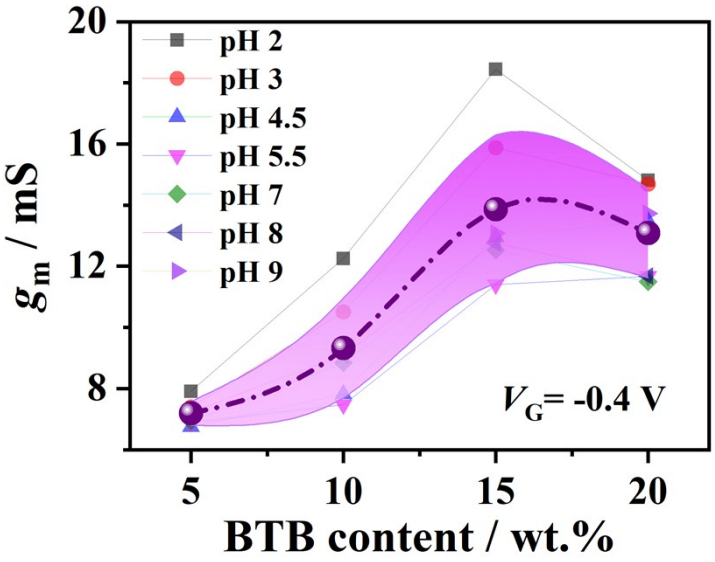

Figure S4 The relationship between transduction and BTB contents at V_G = -0.4 V

6. Reproducibility for the devices

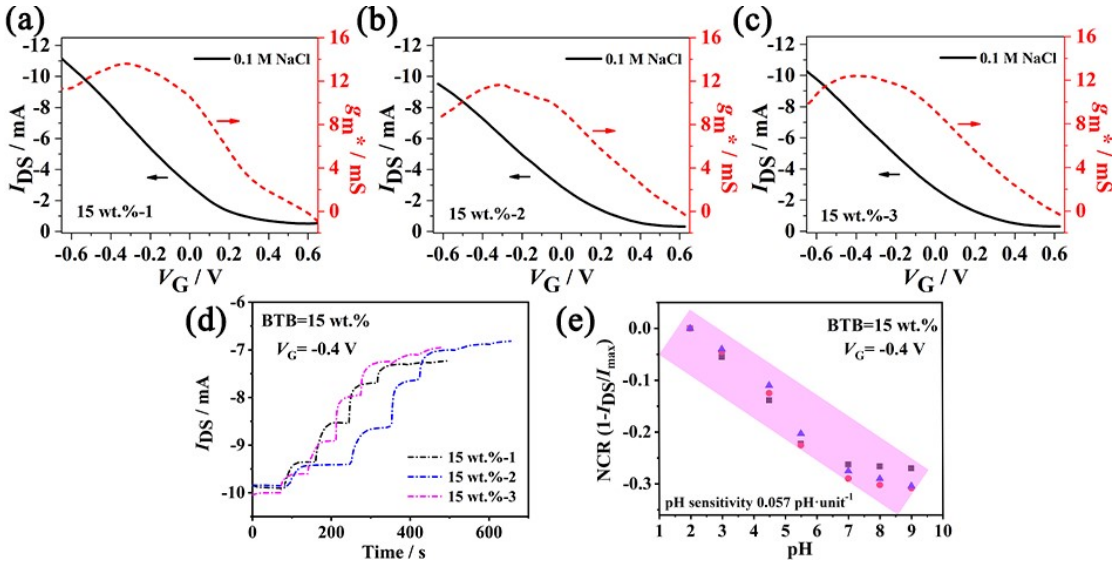

Figure S5 Repeated sensing properties of the device with 15 wt.% BTB at V_G= -0.4 V

7. The X-ray Diffraction patterns

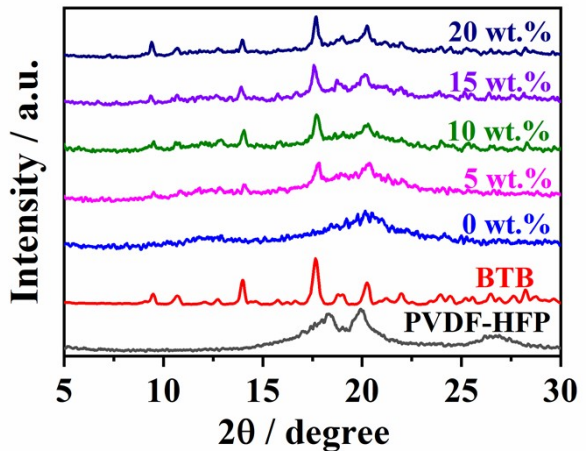

Figure S6 The XRD patterns of ion-gels with different contents in BTB、pure PVDF-HFP powder, and pure BTB powder

8. The crystalline size

Table S2 The crystalline size of PVDF-HFP and BTB in ion-gels with different BTB contents fitted by XRD

BTB content	Particle size / nm	
	PVDF-HFP	BTB
0 wt.%	19	0
5 wt.%	23.4	21.1
10 wt.%	28.1	28.5
15 wt.%	26.8	25.9
20 wt.%	41.3	41.4

9. Element distribution in the ion-gel

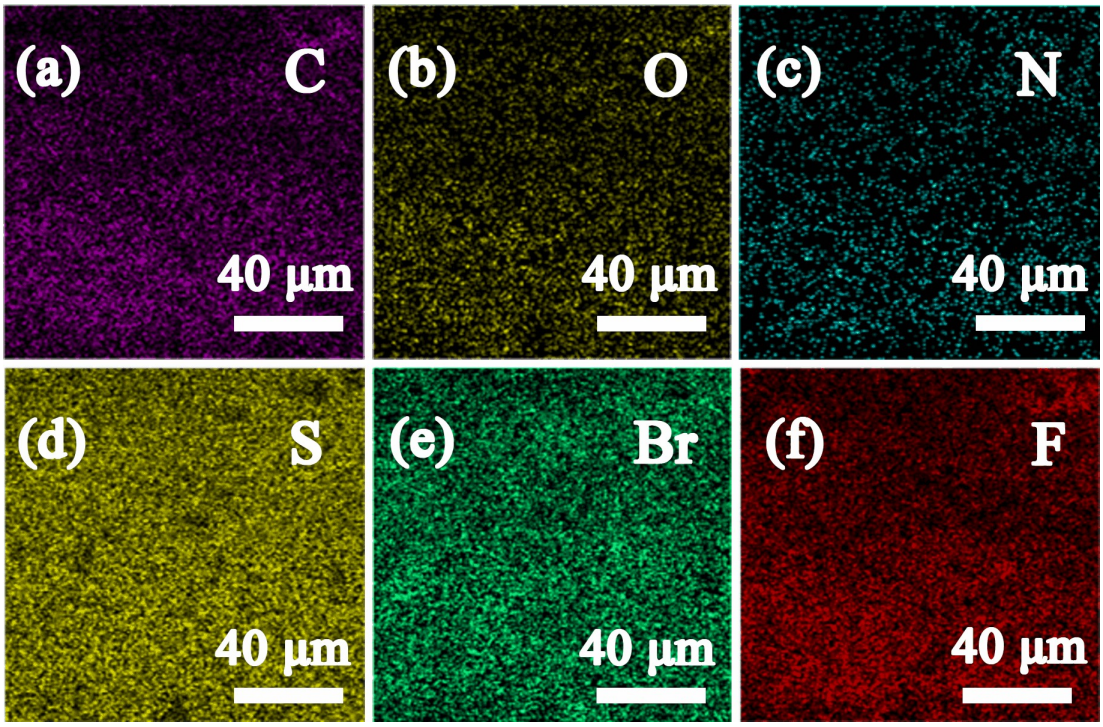

Figure S7 Energy Dispersive Spectroscopy (EDS) elemental mapping of the ion-gel with 20 wt.% BTB

10. The XPS spectra of ion-gel

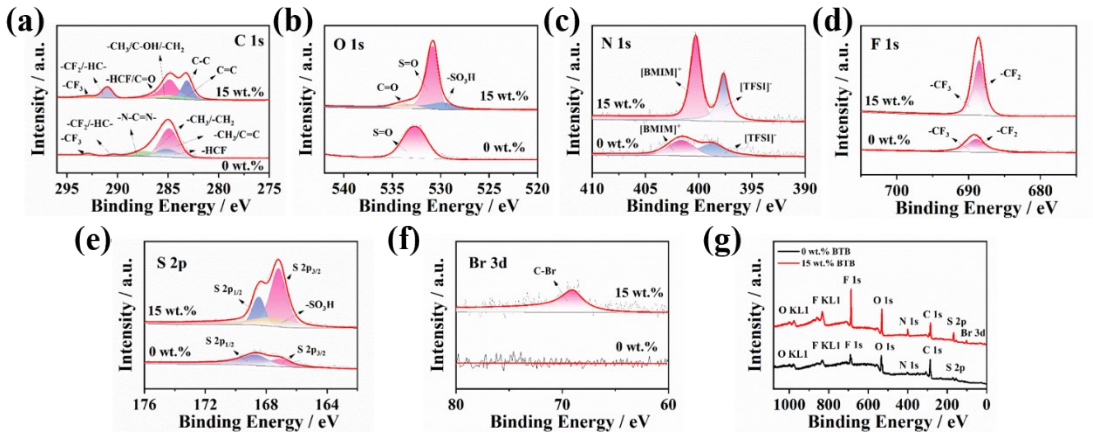

Figure S8 The XPS spectra of Ion-gel with 0 wt.% and 15 wt.% BTB

In this paper, XPS analysis of the PEDOT:PSS channel and ion-gels (0 and 15 wt.% BTB) were performed, respectively. For ease of description, we use 0 BTB and 15 BTB to represent 0 wt.% BTB and 15 wt.% BTB, respectively. In Fig. S8, the ion-gels show typical peaks of Br 3d in addition to the common C1s, O1s, N1s, S2p, and

F1s. Notably, the Br element is derived from the BTB dye molecule [1]. And the N elements are belonging to the [BMIM][TFSI]. The ion-gels (0 and 15 wt.% BTB), due to the presence of PVDF-HFP, and the typical absorption peaks for the -CF_3 group in PVDF-HFP [2] are observed in Fig. S8a.

Moreover, in Fig. 4 of the paper, the XPS spectra of the PEDOT:PSS channel are shown. The C1s, O1s, S2p, F1s, and N1s spectra of the channel can be observed in Figs. 41b-f. In the C1s spectrum of Fig. 4b, the 15 BTB (in pH 2) sample shows three characteristic peaks located at 284.5 eV, 285.12 eV, and 286.6 eV, which are corresponded to the C=C chemical bonding in PEDOT, the C-C chemical bonding in PEDOT [3], and the N-C=C-N bonding in $[BMIM]^+$, respectively [4]. And the chemical state peak of N-C=N in $[BMIM]^+$ located at 287.6 eV has also been observed in alkaline [5]. The relevant peak positions in 0 BTB are slightly shifted. As for the $PEDOT^+$ in the 15/0 BTB under an acidic environment, O1s is at 531.7 eV and 531.9 eV, however, the O1s absorption peaks attributed to the PSS^- are located at 533.6 eV and 533.1 eV, respectively [5]. In addition, there is another absorption peak ascribed to the O1s in $[TFSI]^-$, which appears at 531.09 eV for the 15 BTB sample. The disappearance of the peak corresponding to $[TFSI]^-$ under alkaline conditions indicates that the $[TFSI]^-$ dopant in the channel is out. The fine spectrum of S2p contains peaks from the $PEDOT^+$ and PSS^- are shown in Fig. 4d. The absorption peaks at 170.1 eV and 168.9 eV in the 15 BTB of S2p are attributed to $S2p_{1/2}$ and $S2p_{3/2}$, respectively. The same absorption peaks are located at 170.23 eV and 168.92 eV in the 0 BTB sample. The peaks at 163.7 eV and 165 eV are originated from the PEDOT (15 BTB) [3,4]. The peaks of the -CF_3 group are more visually observed in the F1s fine spectrum, while the $[BMIM]^+$ and $[TFSI]^-$ N1s signals are fitted in Fig. 4f [4]. The N1s peaks in 15 BTB are located at 402.02 eV and 399.51 eV, respectively. From acid to base, the intensity of the peak corresponding to $[BMIM]^+$ increases but that of $[TFSI]^-$ decreases.

11. Time-dependent impedance of ion-gel dielectric layer

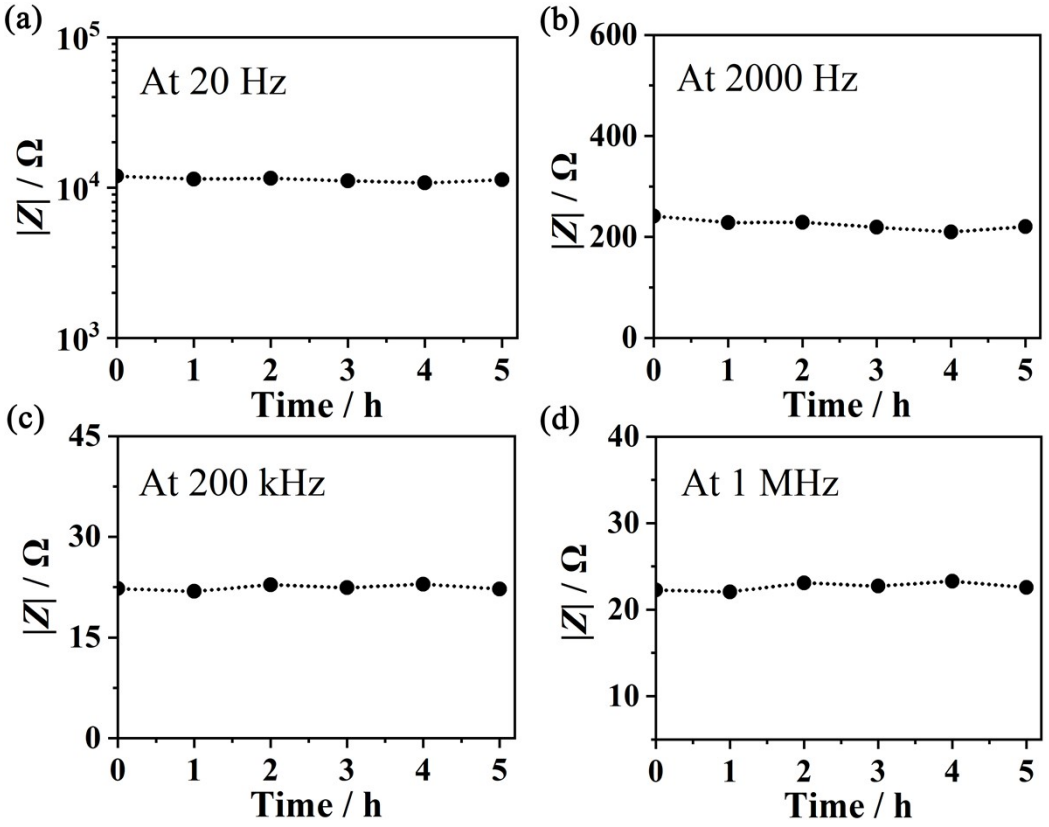

Figure S9 Impedance of the ion-gel as a function of time at (a) 20 Hz, (b) 2000 Hz, (c) 200 kHz, (b) 1 MHz

12. Mechanical properties of flexible chips

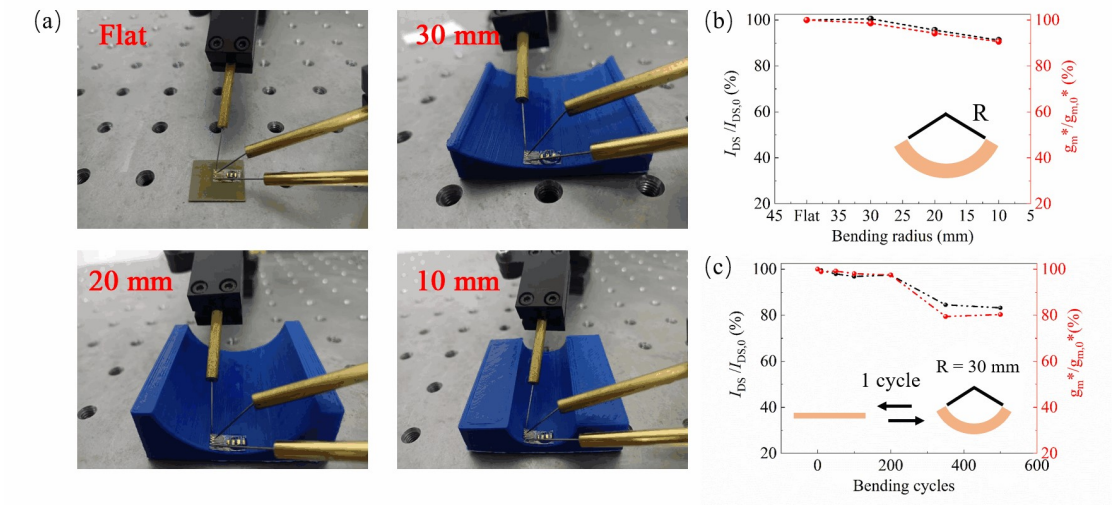

Figure S10 Flexible chip curvature experiments. (a) the optical image of the experimental setup, (b) the current response and peak transduction retention under different curvatures, and (c) the current response and peak transduction retention during durability characterizations.

13. Wettability of the ion-gel in different pH solutions

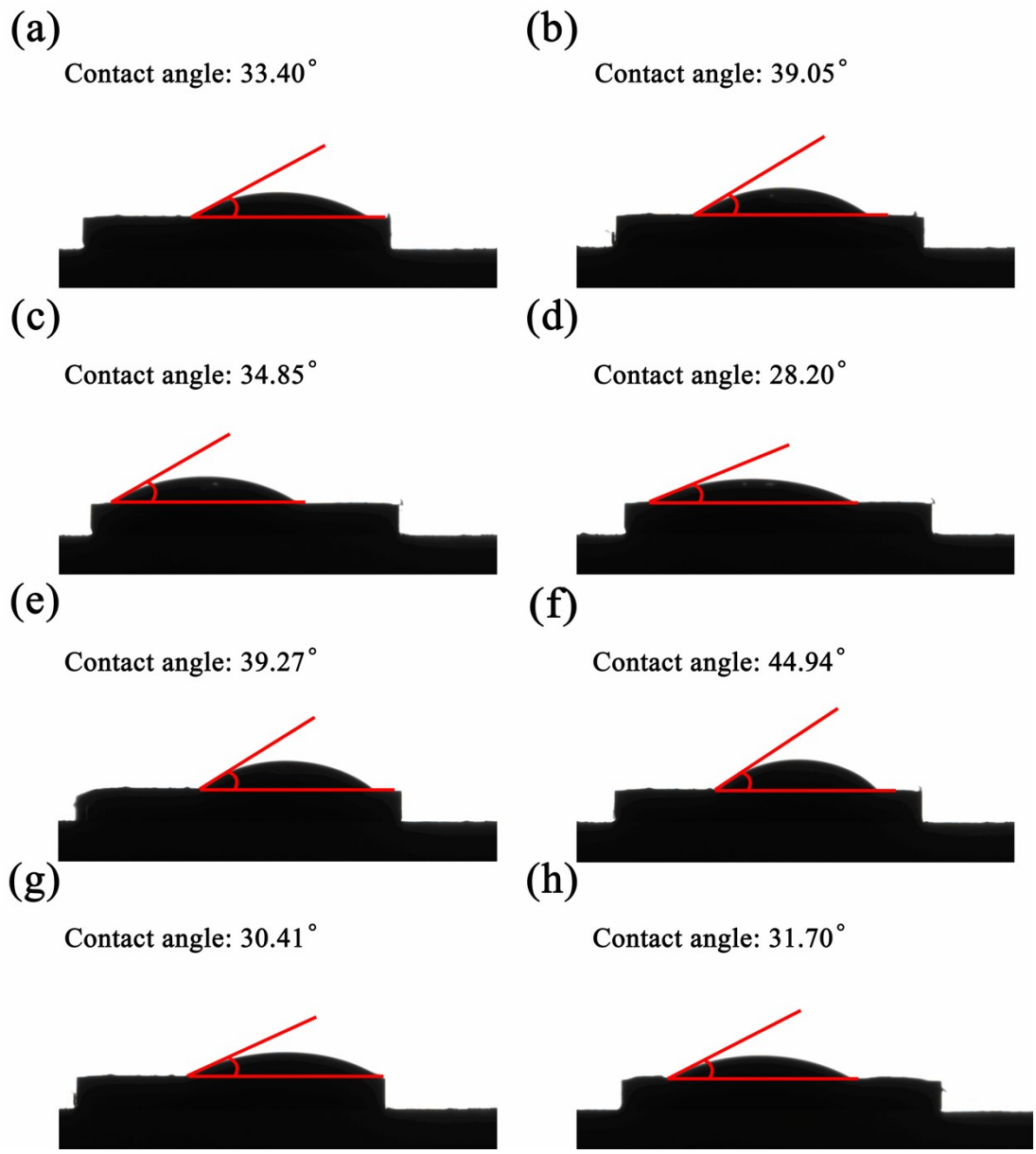

Figure S11 Contact angle of the ion-gel dielectric layer with aqueous solutions of different pH levels. (a, b) pH 3, (c, d) pH 5.5, (e, f) pH 7, and (g, h) pH 9

14. Sensitivity of pH sensors

Table S3 The sensitivity of some flexible pH sensors ($\mu A \cdot dec^{-1}$)

Sensing methods	Dielectric	Sensitive materials	Sensitivity ($\mu A.pH^{-1}$)	Ref.
OECT	Water	PANI	5.25	[6]
OECT	Water	PANI	20	[7]
OECT	Water	IrOx	9.5	[6]
OECT	Water	H^+- ISM	11	[8]
OECT	Water	IrOx	59	[9]
EG-FET	Water	Pt@ZnO	47.82	[10]
Chemical	Hydrogel	Pd/PdO	59 $mV.pH^{-1}$	[11]
OECT	Ion-gel	BTB	91	Our work

1. P. Viswanath and M. Yoshimura, *SN Appl. Sci.*, 2019, **1**, 1-9.
2. X. Gu, S. Bi, L. N. Guo, Y. Q. Zhao and T. S. Li, *ACS omega*, 2017, **2**, 5415-5433.
3. C. T. Chen, Y. L. Yu, K. M. Li, M. Y. Zhao and L. Liu, *Cellulose*, 2015, **22**, 3929-3939.
4. L. Du Hill, M. De Keersmaecker, A. E. Colbert, J. W. Hill, D. Placencia, J. E. Boercker, N. R. Armstrong and E. L. Ratcliff, *Mater. Horiz.*, 2020, **9**, 471-481.
5. L. J. Hu, M. Li, K. Yang, Z. Xiong and B. Yang, *J. Mater. Chem. A*, 2018, **6**, 16583-16589.
6. G. Scheiblin, R. Coppard, R. M. Owens, P. Mailley and G. G. Malliaras, *Adv. Mater. Technol.*, 2017, **2**, 1600141.
7. S. Demuru, B. P. Kunnel and D. Briand, *Biosens. Bioelectron.: X.* 2021, **7**, 100065.
8. S. Demuru, B. P. Kunnel and D. Briand, *Adv. Mater. Technol.*, 2020, **5**, 2000328.
9. F. Mariani, M. Serafini, I. Gualandi, D. Arcangeli, F. Decataldo, L. Possanzini, M. Tessarolo, D. Tonelli, B. Fraboni and E. Scavetta, *ACS Sens.* 2021, **6**, 2366-2377.
10. Y.-L. Chu, S.-J. Young, H.-R. Dai, Y.-M. Lee, A. Khosla, T.-T. Chu and L.-W. Ji, *ECS Journal of Solid State Science and Technology.* 2021, **10**, 067001.
11. V. C. Diculescu, M. Beregoi, A. Evanghelidis, R. F. Negrea, N. G. Apostol and I. Enculescu, *Sci. Rep.*, 2019, **9**, 8902.